https://doi.org/10.5194/egusphere-2024-3180
Preprint. Discussion started: 6 December 2024

What makes the less urbanized city a deeper ozone trap: implications from a case study in the Sichuan Basin, southwest China

Chenxi Wang[1], Zheng Jin[2], Yang Liu[3], Mengxin Bai[4], Weijia Wang[5, 6], Yingzhuo Yu[7], Liantang Deng[8]

[1]Centre for Meteorological Disaster Defence Technology, Sichuan Provincial Meteorological Service, Chengdu 610072, China
[2]College of Geography and Planning, Chengdu University of Technology, Chengdu 610059, China
[3]Key Laboratory of Land Surface Pattern and Simulation, Institute of Geographic Sciences and Natural Resources Research, Chinese Academy of Sciences, Beijing 100101, China
[4]Beijing Municipal Climate Centre, Beijing Meteorological Bureau, Beijing 100089, China
[5]Weather Modification Office of Sichuan Province, Sichuan Provincial Meteorological Service, Chengdu 610072, China
[6]Cloud-Precipitation Physics and Weather Modification Key Laboratory, China Meteorological Administration, Beijing 100081, China
[7]Nanjing Institute of Environmental Sciences, Ministry of Ecology and Environment, Nanjing 210042, China
[8]CMA Earth System Modelling and Prediction Centre, China Meteorological Administration, Beijing 100081, China

Correspondence to: Zheng Jin (zjin@cdut.edu.cn)

Abstract. The urban-rural gradient of surface ozone concentration is widely reported in global megacities. As yet, quantitative analyses for this gradient pattern have been lacking. Using near surface atmospheric pollutant reanalysis and remote sensing measurements, we demonstrate a dipole-like urban surface ozone trap pattern in two megacities (Chengdu and Chongqing) in the Sichuan Basin. During the study period of 2013-2019, the urban-rural gradients of surface ozone level in Chongqing were higher than in Chengdu despite Chongqing's lower urbanization level. In winter, the ozone level in the core area of Chongqing/Chengdu is 16.4/22.1 μg m^{-3}, with an increasing rate of 8.98%/5.19% per 10 km towards the surrounding suburban area. However, the nitrogen dioxide level in Chengdu is higher than in Chongqing. Besides, the concentration levels of formaldehyde and ultraviolet-absorbing aerosol did not show comparable differences between these two cities. Regarding the meteorological conditions, atmospheric visibility, sunshine duration, and nighttime wind speed in Chongqing were all lower compared to Chengdu, the ozone trap pattern aligns more with meteorological condition rather than chemical condition. Our study characterized the ozone trap pattern for two megacities with different urbanization levels, providing a novel perspective on urban atmospheric environment assessment.

Highlights

1. A dipole-like spatial pattern of near surface ozone trap across two megacities of the Sichuan Basin is demonstrated via air quality reanalysis during 2013-2019.
2. Chongqing has the deeper ozone trap compared to Chengdu despite its lower urbanization level.
3. The ozone trap pattern aligns more closely with meteorological condition rather than chemical condition.

https://doi.org/10.5194/egusphere-2024-3180
Preprint. Discussion started: 6 December 2024

1. Introduction

Ozone (O_3) in the near-surface atmosphere is a secondary pollutant, formed from oxides of nitrogen (NO_x) and volatile organic compounds (VOCs) as precursors (Sillman, 1999). Anthropogenic NO_x emissions include nitrogen monoxide (NO) and nitrogen dioxide (NO_2). In ambient atmosphere, NO_2 can produce O_3 via photolysis with VOCs (Kleinman, 1994; Lelieveld and Dentener, 2000). Conversely, the NO can deplete the O_3 by titration (Murphy et al., 2007). The O_3 is a major oxidant for the trace gases in the atmosphere that can promote a variety of free radical chain reactions, and it is also a pivotal greenhouse gas (Mickley et al., 1999; Unger et al., 2006; Monks et al., 2015; Liu et al., 2022). Further, the O_3 has damaging impacts on human health, terrestrial vegetation, and crops (Anenberg Susan et al., 2012; Tai et al., 2014; Lelieveld et al., 2015; Yue et al., 2017). In China, near-surface atmospheric O_3 pollution is likely to be a more serious issue. Site observations from 74 Chinese cities revealed that the number density of ozone in daily max-8-hour has increased from 69.5 to 75.0 (ppbv) during 2013-2015 (Wang et al., 2017). Surface ozone level is also found to be enhanced from 2013-2014 to 2016-2017 in China (Lu et al., 2018). Projections based on climate and emission changes indicated that ozone pollution is likely to be more severe in China (Wang et al., 2013).

Understanding the mechanisms behind multi-year normal surface O_3 levels is crucial for ozone pollution research. Indeed, previous studies have highlighted the discrepancy in surface O_3 levels between urban and rural areas. Using observations from 1497 sites, surface O_3 levels are found lower in urban areas than in rural over China (Zhang et al., 2020). Similar low to high discrepancies of O_3 levels from urban to rural are also found in U.S.A, Spain, U.K, and Turkey (Stasiuk and Coffey, 1974; Dueñas et al., 2004; Atkinson Richard et al., 2012; Im et al., 2013; Betancourt-Odio et al., 2021). In Europe, the urban O_3 is increasing faster than in rural areas (Yan et al., 2019). In the Sichuan Basin, satellite-based observation demonstrated a basin-wide increase long-term O_3 trends during 2013-2020 (Wu et al., 2022). Regarding the spatial analysis of surface O_3 level in the Sichuan Basin, current studies have revealed comprehensive spatial-temporal patterns through site-based observations (Zhao et al., 2018; Fang et al., 2021). Due to the heterogeneity of the site distribution, the spatial analyzability of surface pollutants directly observed from air quality monitoring sites is relatively inefficient. Nevertheless, satellite observations can be representative of the entire tropospheric atmosphere, which may differ from the condition of the near surface (Veefkind et al., 2012). Previous studies have characterized the spatial patterns of surface ozone level over the Sichuan Basin using site observations (Zhao et al., 2019; Ning et al., 2020; Deng et al., 2022), model simulations (Wu et al., 2022), and machine learning estimations (Liu et al., 2020). However, site-based observations alone cannot provide a comprehensive view of the ozone spatial pattern, as comparisons between different regions can only be made using roughly defined locations. For example, Ning et al. (2020) categorized the sites into two groups: the eastern and western basin. In a model simulation study, Wu et al. (2022) presented spatial patterns of April-August average ground-level ozone concentration over the Sichuan Basin. They indicated that the predicted low levels of O_3 in the core area of Chengdu and Chongqing in 2016 were primarily caused by NO titration, which aligns with ground-level ambient observations. Since the simulation results for 2019 and 2020 did not show prominent ozone traps anymore, the O_3 traps in 2016 are regarded as an

https://doi.org/10.5194/egusphere-2024-3180
Preprint. Discussion started: 6 December 2024

episodic event. However, by presenting the ozone pattern of a 7-year-long average, we revealed the trap pattern of near surface ozone was a long-term normal status. Finally, we further presented a quantified analysis for the urban-rural gradients, which has not been addressed in previous studies. To address these gaps, we utilize a 7-year-long air pollutants reanalysis (**section 2.3**) to characterize the surface spatial patterns. Then, we illustrated the relationship between pollutant concentration and urbanization level using satellite-based high-resolution land surface cover data (**section 2.2**). Our analysis of the urban-rural concentration discrepancy in the Sichuan Basin revealed the phenomenon of surface O_3 trapping in the highly urbanized city core area. These results can enhance our understanding of the source-sink dynamics and key factors affecting surface O_3 level.

2. Method

2.1 Study area

The Sichuan Basin is the largest low-lying basin in China, located on the southeastern margin of the Tibetan Plateau, covering an area of approximately 2.6×10^5 km^2 and home to over 110 million people. The Chengdu-Chongqing urban agglomeration is surrounded by mountains around the Sichuan Basin. Chengdu and Chongqing, situated in the northwest and southeast of the Sichuan Basin, serve as vital transportation hubs and economic centers in western China. The topography of the Sichuan Basin often causes atmospheric stagnation in the near-surface layer, leading to severe pollution events due to pollutant accumulation (Liao et al., 2018; Cao et al., 2020). Satellite-born datasets, including Global Multi-Resolution (30~225 m) Terrain Elevation Data 2010 (GMTED2010) (Danielson and Gesch, 2011) (https://www.usgs.gov/coastal-changes-and-impacts/gmted2010) and Moderate Resolution Imaging Spectroradiometer (MODIS) land cover data (Friedl and Sulla-Menashe, 2019) (https://modis.gsfc.nasa.gov/data/dataprod/mod12.php), were utilized to exhibit the geospatial pattern of Sichuan Basin. Chengdu and Chongqing are situated in the northwest and southeast of the Sichuan Basin, respectively, with other minor cities evenly distributed between them. In terms of land cover type, Chengdu and Chongqing have the largest and most concentrated urban areas within the Sichuan Basin, with the plains surrounding the cities being mainly cropland, while the surrounding mountainous areas are mainly grassland and forest (**Figure 1a, b**). To define the study region, we resampled GMTED2010 data to 1 km × 1 km at a lower resolution via the algorithm of LAF (largest area fraction) under CDO (Climate Data Operator, https://code.mpimet.mpg.de/projects/cdo). Then, we filtered out each pixel in case the averaged elevation within a 15-km radius centered on it exceeded 600 m, and finally removed any pixels over 700 m. This process delineated the study area within the Sichuan Basin, encompassing its low-altitude regions. (**Figure 1a**).

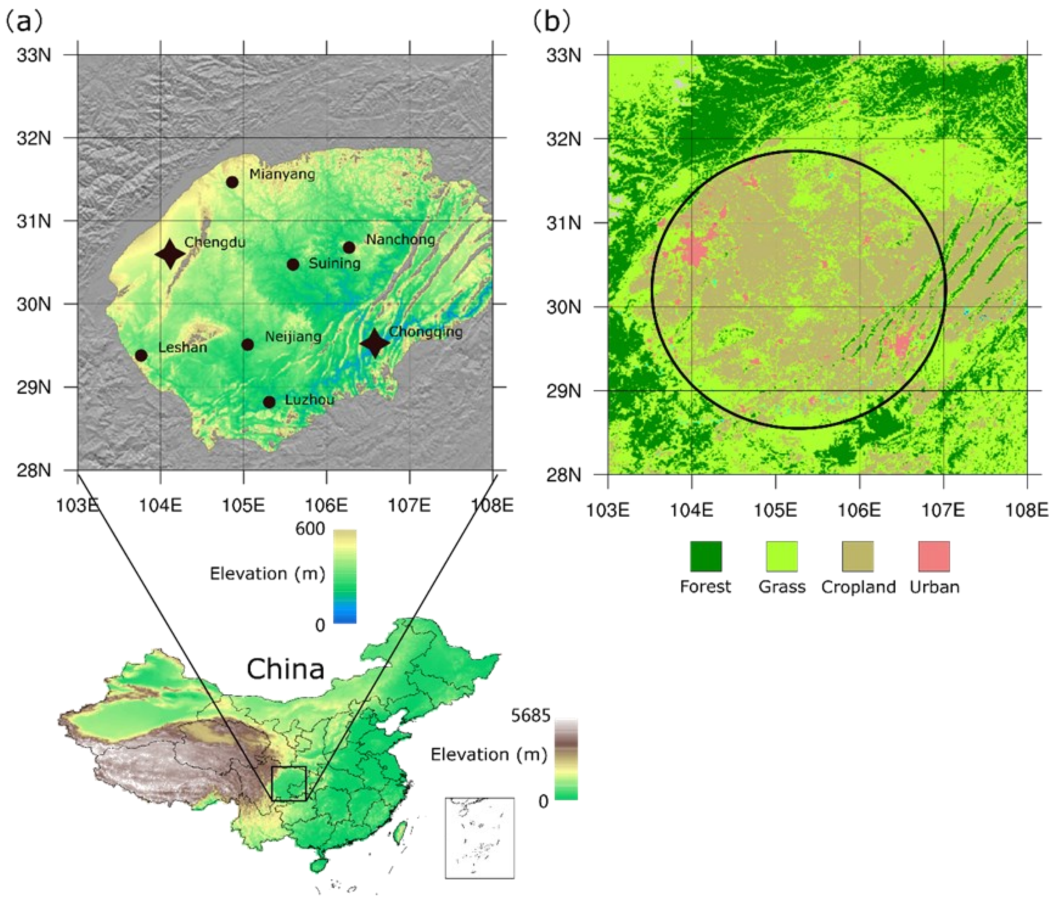

95 **Figure 1: Geographical information of the study area. (a) Location of the Sichuan Basin with major cities. (b) Spatial pattern of land cover types.**

2.2 Evaluation of urbanization level

The global annual impervious area (GAIA) data (Gong et al., 2020; Li et al., 2020) (https://developers.google.com/earth-engine/datasets/catalog/Tsinghua_FROM-GLC_GAIA_v10) are utilized to assess the urbanization level of the cities. In the definition of GAIA data, the impervious areas include multiple artificial land surface objects, such as roofs, road surfaces, hardened grounds, etc. The satellite-based GAIA dataset has a raw horizontal resolution of 30 m and span from 1985 to 2018. The process of urbanization revealed by the GAIA dataset is generally consistent, showed an average overall accuracy exceeded 90% (Gong et al., 2020). Based on the GAIA data (in 30 m resolution), we calculated the fraction of impervious surface area (ISA) in each 1 km pixel. Since the GAIA data represent the final ISA values for one year, it is preferable to assess the impact of urbanization in current year by using the data from last year. Therefore, we used the GAIA data during 2012-2018 in our study. **Figure 2** displayed a comparison of ISA fraction spatial patterns between 2012 and 2018 in the study area. Generally, the urbanization changes revealed by the GAIA data during this 7-year period are substantially increases in density rather than spatial expansions.

https://doi.org/10.5194/egusphere-2024-3180
Preprint. Discussion started: 6 December 2024

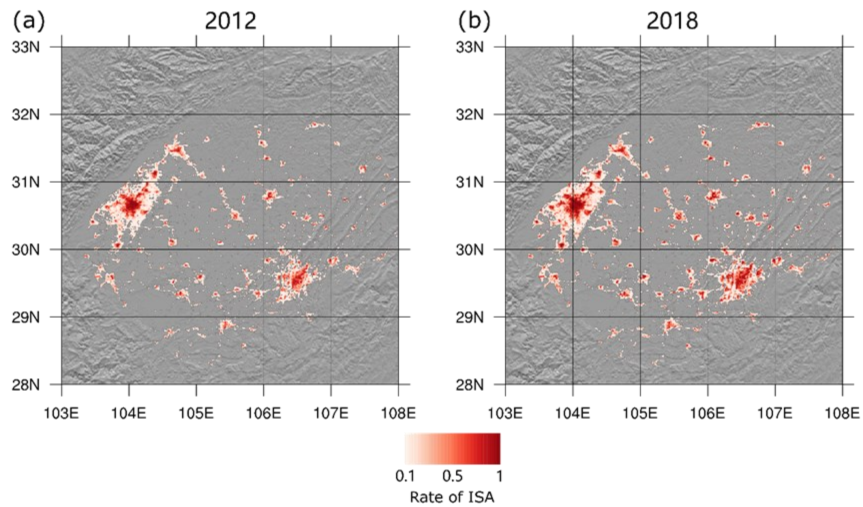

Figure 2: Spatial patterns for the rate of Impervious Surface Area (ISA) in 2012 (a) and 2018 (b) in the study area of Sichuan Basin.

2.3 Datasets for air pollutants

The Chinese air quality reanalysis (CAQRA, https://www.scidb.cn/en/detail?dataSetId=712258947691577344) is a high-resolution dataset generated by assimilating observations from over 1400 sites. All of these sites are under the China National Environmental Monitoring Centre (CNEMC). The featured assimilation techniques utilized in CAQRA are ensemble Kalman filter (EnKF) and Nested Air Quality Prediction Modeling System (NAQPMS) (Kong et al., 2021). The CAQRA provides gridded concentrations of ground surface air pollutants, including $PM_{2.5}$, PM_{10}, sulfur dioxide (SO_2), NO_2, carbon monoxide (CO), and O_3. The accuracy of CAQRA has been evaluated through cross-validation, yielding a root mean square error (RMSE) of 14.4 μg m^{-3} for monthly O_3 concentration. and 12.6 μg m^{-3} for monthly NO_2 concentration. We used the 7-year-long (2013-2019) average for seasons: March-April-May for spring, June-July-August for summer, September-October-November for autumn, December-January-February for winter. To maintain a consistent resolution with GAIA and elevation datasets, and enhance spatial analyzability, we resampled the CAQRA data to a horizontal resolution of 1 km × 1 km via the LAF algorithm under CDO. In terms of satellite-based pollutant measurements, including ozone, nitrogen dioxide, formaldehyde, we utilized Sentinel-5P data (https://dataspace.copernicus.eu/explore-data/data-collections/sentinel-data/sentinel-5p).

2.4 Meteorological datasets

The atmospheric visibility and sunshine duration are derived from auto meteorology stations around the urban regions of Chengdu and Chongqing. There are 7 sites around Chengdu city, including Wenjiang (30.74°N, 103.86°E), Chongzhou (30.68°N, 103.70°E), Pidu (30.81°N, 103.88°E), Xinjin (30.45°N, 103.81°E), Longquanyi (30.61°N, 104.26°E), Xindu (30.77°N, 104.18°E), and Jintang (30.81°N, 104.42°E). Besides, there are 5 sites around Chongqing city, including Yubei

https://doi.org/10.5194/egusphere-2024-3180
Preprint. Discussion started: 6 December 2024

(29.73°N, 106.61°E), Bishan (29.58°N, 106.21°E), Shapingba (29.57°N, 106.46°E), Jiangjin (29.28°N, 106.25°E), and Banan (29.33°N, 106.50°E). Based on the average of multiple sites around each city, we derived 7-year-long (2013-2019) seasonal visibility (m) and sunshine duration (hours) in Chengdu and Chongqing. These visibility and sunshine duration observations can be used as a direct assessment for the visible light in the near-surface atmosphere. For the near surface wind data, we used ERA5-Land (Muñoz-Sabater et al., 2021) (https://cds.climate.copernicus.eu/cdsapp#!/dataset/reanalysis-era5-land), which represents the wind speed at 10 m height. Finally, we used satellite-based MODIS-Aqua data for the measurement of land surface temperature (LST) (https://modis.gsfc.nasa.gov/data/dataprod/mod11.php).

2.5 Analysis of the urban-rural gradients

First, we identified the core points of Chengdu and Chongqing, approximating the central squares (Tianfu square and Jiefangbei square) within 1 km × 1 km pixels. Then, we generated the map of radius distance centered to the city's core area over our study region (**Figure A1**). Using this map, we determined the reference value by averaging values within a 5-km radius centered to the city core. Based on this reference value, we can derive the relative levels of ISA fraction, O_3, and NO_2 at each 1-km interval departing away to the city core. This spatial analysis method can be referred to a previous study by Zhang et al. (2022).

3. Results

3.1 Response of pollutant concentration to urbanization level

Throughout the study area, Chengdu has the largest ISA fraction (83.1%), followed by Chongqing (64.9%). The other cities have smaller ISA fractions, all below 50%, and distributed dispersedly in the Sichuan Basin (**Figure 2**). The spatial patterns of near surface O_3 level varies a lot with the seasons. Averaged during 2013-2019, the highest O_3 level is observed in summer (73.1 μg m^{-3}), followed by spring (62.7 μg m^{-3}), autumn (44.1 μg m^{-3}), and winter (35.7 μg m^{-3}). In terms of the spatial pattern, the O_3 level in all seasons, exhibited two low centers located at Chengdu (22.1~51.3 μg m^{-3}) and Chongqing (16.4~56.0 μg m^{-3}). These two low centers are more pronounced in autumn (27.4 μg m^{-3}) and winter (43.6 μg m^{-3}) compared to spring (51.3 μg m^{-3}) and summer (60.7 μg m^{-3}) (**Figure 3, Table 1**). Regarding NO_2 level, the seasons in the study area follow a descending order from high to low: winter (29.0 μg m^{-3}), autumn (22.3 μg m^{-3}), spring (21.7 μg m^{-3}), and summer (17.0 μg m^{-3}). Besides, there are two high NO_2 centers located at Chengdu (34.5~48.6 μg m^{-3}) and Chongqing (28.7~38.1 μg m^{-3}). For all seasons, the high NO_2 center at Chengdu is higher compared to Chongqing (**Figure 4, Table 1**).

https://doi.org/10.5194/egusphere-2024-3180
Preprint. Discussion started: 6 December 2024

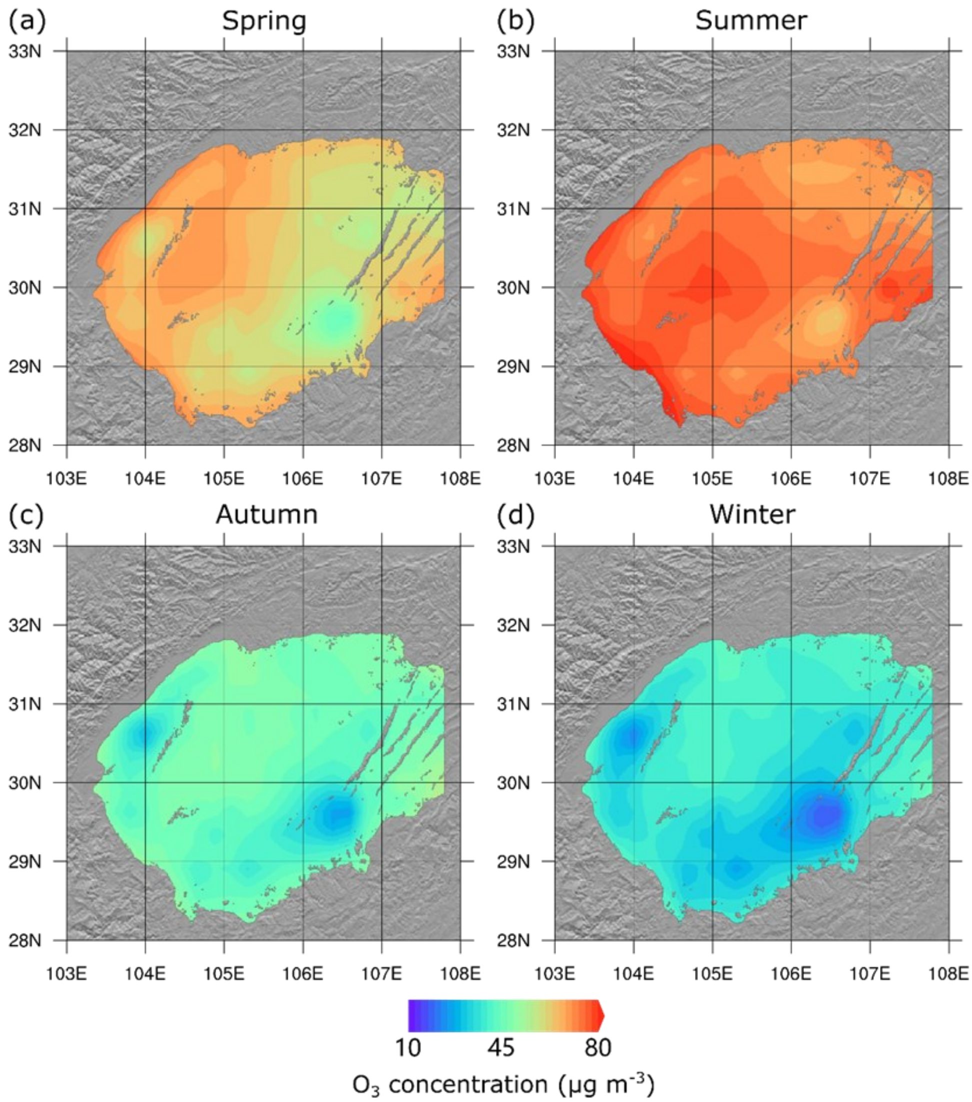

155 **Figure 3: Spatial patterns for ozone (O_3) concentrations over seasons during 2013-2019.**

https://doi.org/10.5194/egusphere-2024-3180
Preprint. Discussion started: 6 December 2024

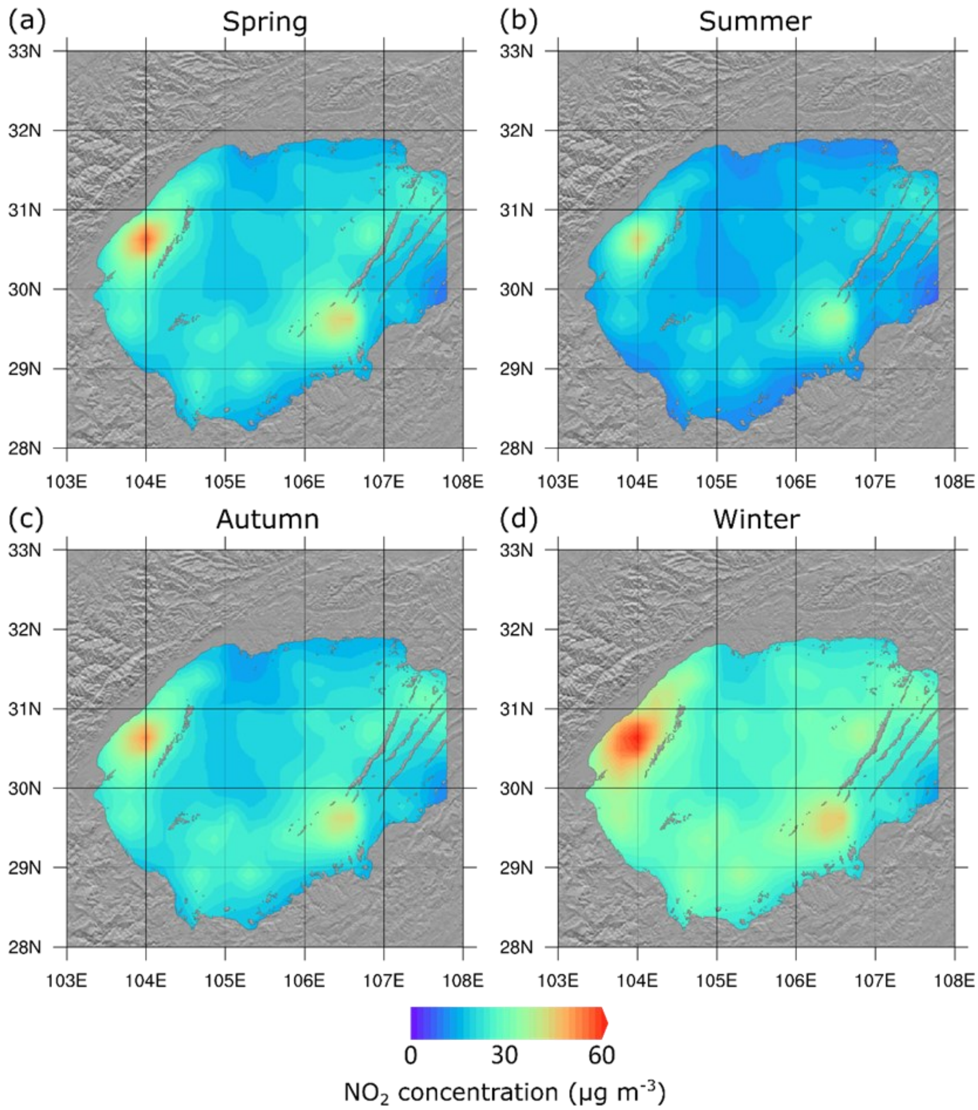

Figure 4: Spatial patterns for nitrogen dioxide (NO_2) concentrations over seasons during 2013-2019.

Table 1: Averaged concentrations within 5-km radius centered to the core area and the urban-rural gradients of relative O_3 and NO_2 levels.

City	Pollutant	Season							
		Spring		Summer		Autumn		Winter	
		core	slope	core	slope	core	slope	core	slope
Chengdu	O_3	51.3	1.29	60.7	0.61	27.4	4.91	22.1	5.19
	NO_2	43.5	-6.32	34.5	-6.45	40.2	-6.13	48.6	-5.48
Chongqing	O_3	39.4	3.77	56.0	1.63	23.6	6.52	16.4	8.98
	NO_2	35.4	-5.52	28.7	-5.56	35.0	-5.17	38.1	-4.21

Note: Values on the left side are core concentrations (μg m^{-3}), while on the right side are concentration slopes (% $10km^{-1}$), representing the variability of O_3, NO_2 concentrations for every incremental 10 km radius distance centered to the city's core area.

https://doi.org/10.5194/egusphere-2024-3180
Preprint. Discussion started: 6 December 2024

To illustrate the linkage between pollutant concentration and urbanization level, we aggregated the mean concentrations across ISA fraction bins from 0.1~0.2 to >0.8 for both O_3 (**Figure 5**) and NO_2 (**Figure 6**). Generally, mean O_3 levels decrease with increasing ISA fraction in all seasons, while NO_2 levels exhibit the opposite trend. Specifically, from highest to lowest ISA bins, the O_3 levels ranged from 61.8 to 58.8 μg m^{-3} in spring, 72.4 to 70.8 μg m^{-3} in summer, 41.0 to 36.9 μg m^{-3} in autumn, and 32.8 to 29.3 μg m^{-3} in winter. Oppositely, the NO_2 levels ranged from 27.4 to 34.5 μg m^{-3} in spring, 21.1 to 27.1 μg m^{-3} in summer, 27.5 to 33.7 μg m^{-3} in autumn, and 35.1 to 41.2 μg m^{-3} in winter. In autumn and winter, the O_3 level has a wider range at higher ISA bins, indicating more significant concentration differences between highly urbanized areas. However, in spring and summer, the widest concentrations range is corresponding to ISA bin of 0.6~0.8. When the ISA bin are >0.8, the concentration range is narrowed (**Figure 5**). The range of O_3 level is widen by letting down the lower quartile (**Figure 5c-d**), it indicates that low values become lower while high values are relatively constant. These results indicate that in cold seasons (autumn and winter), only a certain part of the highly urbanized areas experienced a significantly lower O_3 level. Typically, O_3 levels are more than twice as high in summer (70.8~72.4 μg m^{-3}) as in winter (29.3~32.8μg m^{-3}). In contrast, the NO_2 levels are higher in winter (35.1~41.2 μg m^{-3}) than in summer (21.1~27.1 μg m^{-3}). Throughout all seasons, the NO_2 levels are increasing with the rise of the ISA fraction, and the concentration range became wider in higher ISA fraction bins (**Figure 6**). The widening concentration range implies that only specific high ISA fraction areas experience significantly higher NO_2 levels. T Hence, the divergent responses of O_3 and NO_2 to ISA fraction indicate that concentration changes are not solely aligned with the ISA level. Alternatively, prominent concentration variations occurred in regions where the high ISA areas were aggregated, such as Chengdu and Chongqing.

https://doi.org/10.5194/egusphere-2024-3180
Preprint. Discussion started: 6 December 2024

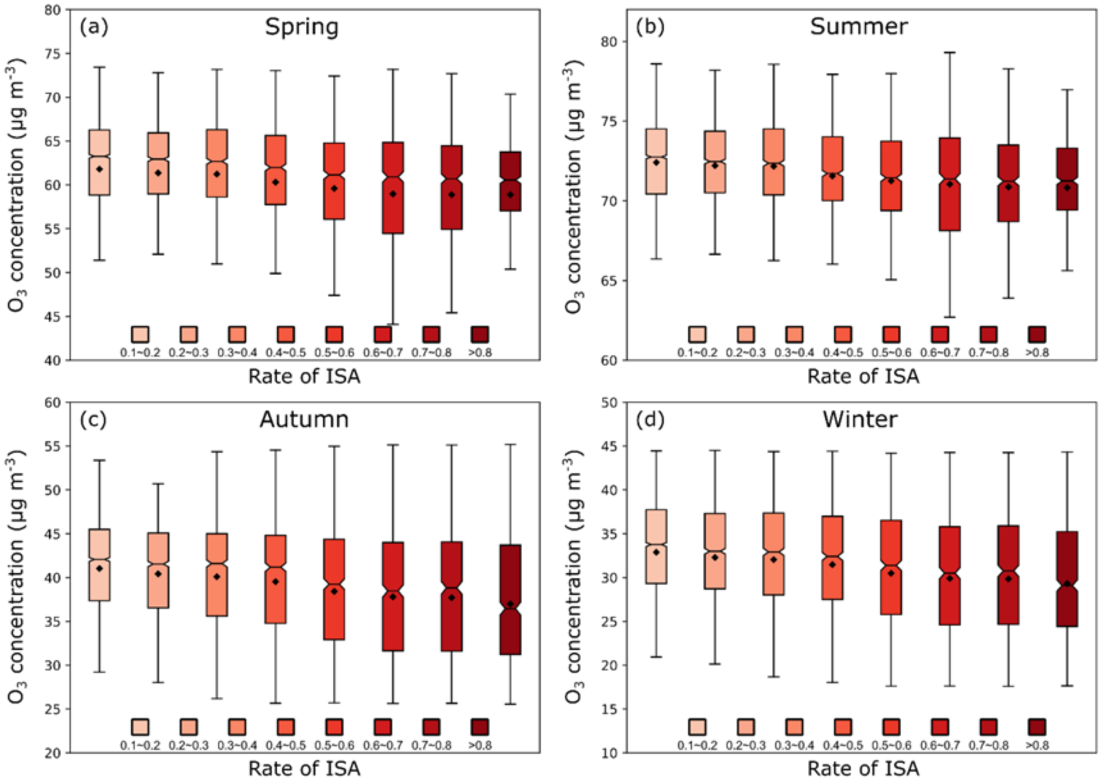

190 **Figure 5: Response of mean O_3 concentration to rate of ISA over seasons during 2013-2019. The solid lines in the mid of the boxes are medians, the notches are the 95% confidence interval of the medians, the black dots are mean values, and the whiskers are interquartile ranges.**

https://doi.org/10.5194/egusphere-2024-3180
Preprint. Discussion started: 6 December 2024

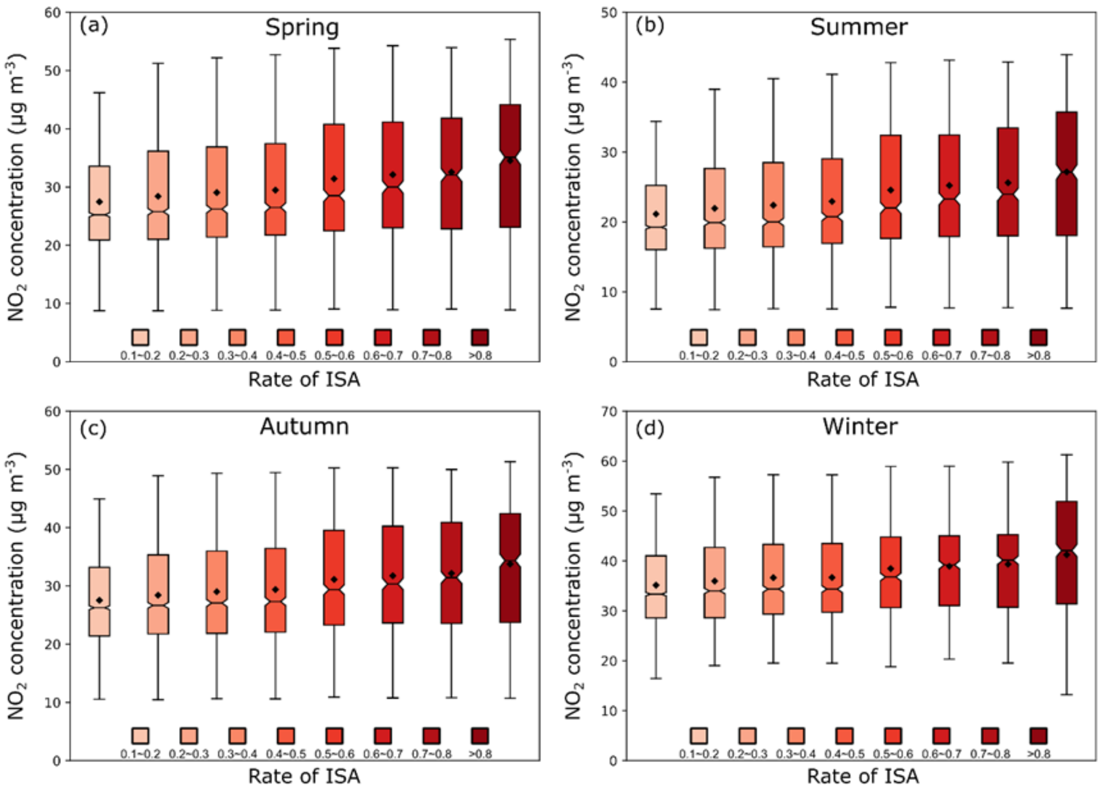

Figure 6: Response of mean NO_2 concentration to rate of ISA over seasons during 2013-2019. The solid lines in the mid of the boxes are medians, the notches are the 95% confidence interval of the medians, the black dots are mean values, and the whiskers are interquartile ranges.

3.2 Characterize the urban ozone trap

Low O_3 levels in the urban core area can result from NO titration (Wu et al., 2022). Here, we briefly illustrate a hypothetical mechanism of urban O_3 trapping (**Figure 9**). Since we focus on the two megacities in the Sichuan Basin, we employ a more direct method to characterize the urban-rural gradient of O_3 and NO_2 levels. First, the urbanization levels both in Chengdu and Chongqing are compared through the ISA proportions. Along with the distance bins from the city core areas to surrounding rural areas, the mean ISA proportions are shown (**Figure 7**). In an average within a 5-km radius centered to the core area, the ISA proportion of Chengdu is over 80%, while for Chongqing is merely over 60%. This 20% difference in ISA persists along the core distance from 5 to 20 km. Beyond a distance of 30 km, ISA proportion decreases to 20% or lower for both Chengdu and Chongqing. In terms of the ISA change from 2012 to 2018, the enhancement is at least 5% within a distance of 10~30 km for Chengdu, and 10~35 km for Chongqing. Both the old urban areas within a 10-km distance and the suburban areas of 30 km away are relatively insignificant in terms of ISA increase. Therefore, averaged within a 30-km distance from the city core area, the urbanization level of Chengdu (35.8%) is higher than Chongqing (25.9%) in terms of ISA fraction.

https://doi.org/10.5194/egusphere-2024-3180
Preprint. Discussion started: 6 December 2024

Regarding relative concentrations, O_3 exhibits upward trends with increasing distance from the city core areas, while NO_2 shows the opposite downward trends (**Figure 8**). When comparing the seasons, O_3 level increases most rapidly with distance during winter, followed by autumn, spring, and summer, while NO_2 level decreases most rapidly with distance in summer, followed by spring, autumn, and winter. In terms of the urban-rural gradient, during winter, the O_3 concentration in Chengdu exceeds 130% at a distance of 40 km, and further exceeds 140% at 80 km or beyond (**Figure 8a**). In Chongqing, the winter O_3 gradient is more pronounced. O_3 exceeds 140% at a distance of 40 km, and approaches 180% at 100 km (**Figure 8b**). In contrast to O_3, the urban-rural gradient of NO_2 level is the opposite. NO_2 decreases more rapidly with the increase of distance in Chengdu compared to Chongqing. At the distance of 100 km in summer, the relative NO_2 concentration is 40% in Chengdu, and 50% in Chongqing (**Figure 8c-d**). Specifically, **Table 1** displays urban core area concentrations and urban-rural gradients for O_3 and NO_2. As reference values, O_3 and NO_2 levels within a 5-km radius centered to the city core area varied pronouncedly over seasons. The core area level of O_3 in Chengdu's summer is 60.7 μg m^{-3}, while in winter is 22.1 μg m^{-3}, representing a decrease of over 60%. In Chongqing, the O_3 level drops over 70% from summer to winter (from 56 to 16.4 μg m^{-3}). In addition, 16.4 μg m^{-3} is the lowest core area O_3 level among all seasons as well as the whole study area. The discrepancy over seasons for the core area level of NO_2 is relatively smaller compared to O_3. From summer to winter, the range is 34.5~48.6 μg m^{-3} for Chengdu, and 28.7~38.1 μg m^{-3} for Chongqing. Urban-rural gradients are presented as enhancement/decay rates (slopes) (**Table 1**). For every 10 km away from the city core area, winter O_3 level increased by 5.19% in Chengdu, and 8.98% in Chongqing. In contrast, during summer, these rates were 0.61% (Chengdu) and 1.63% (Chongqing). Correspondingly, in winter, the slopes of NO_2 levels are 5.48% (Chengdu) and 4.21% (Chongqing), while in summer are 6.45% (Chengdu) and 5.56% (Chongqing). Since the urban traffic emits NO_x with a substantial portion of NO (Zhou et al., 2014; Hagenbjörk et al., 2017), the urban NO titration played a key role in trapping the O_3 (Murphy et al., 2007). Therefore, since these levels and gradients are ambient statuses based on a 7-year long average (2013-2019), and considering the inversed spatial patterns in O_3 and NO_2 levels, the O_3 trap pattern are related to the NO titration induced by urban vehicle emissions. However, Chongqing has a deeper O_3 trap at lower NO_2 level compared to Chengdu. Since the NO is proportional to NO_2 in traffic-related NO_x emissions, there should be other factors contributing to the disparity in strength of O_3 trapping under NO titration.

https://doi.org/10.5194/egusphere-2024-3180
Preprint. Discussion started: 6 December 2024

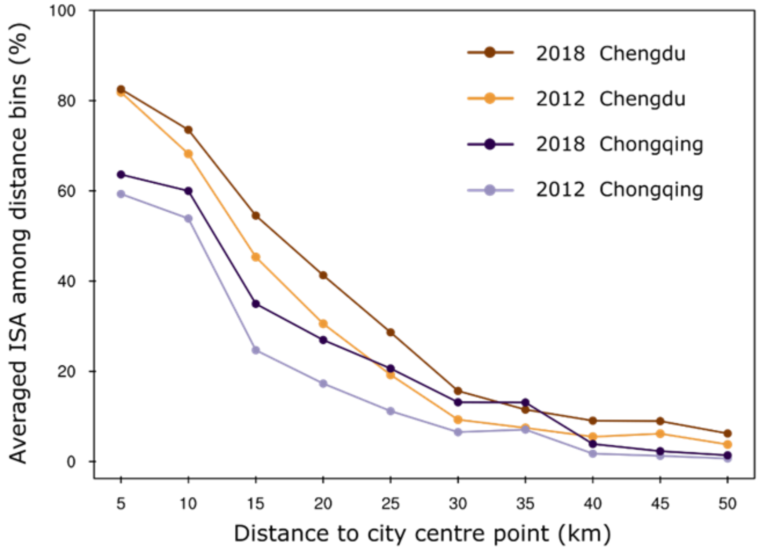

Figure 7: The average rates of ISA among distance bins for Chengdu and Chongqing in 2012 and 2018.

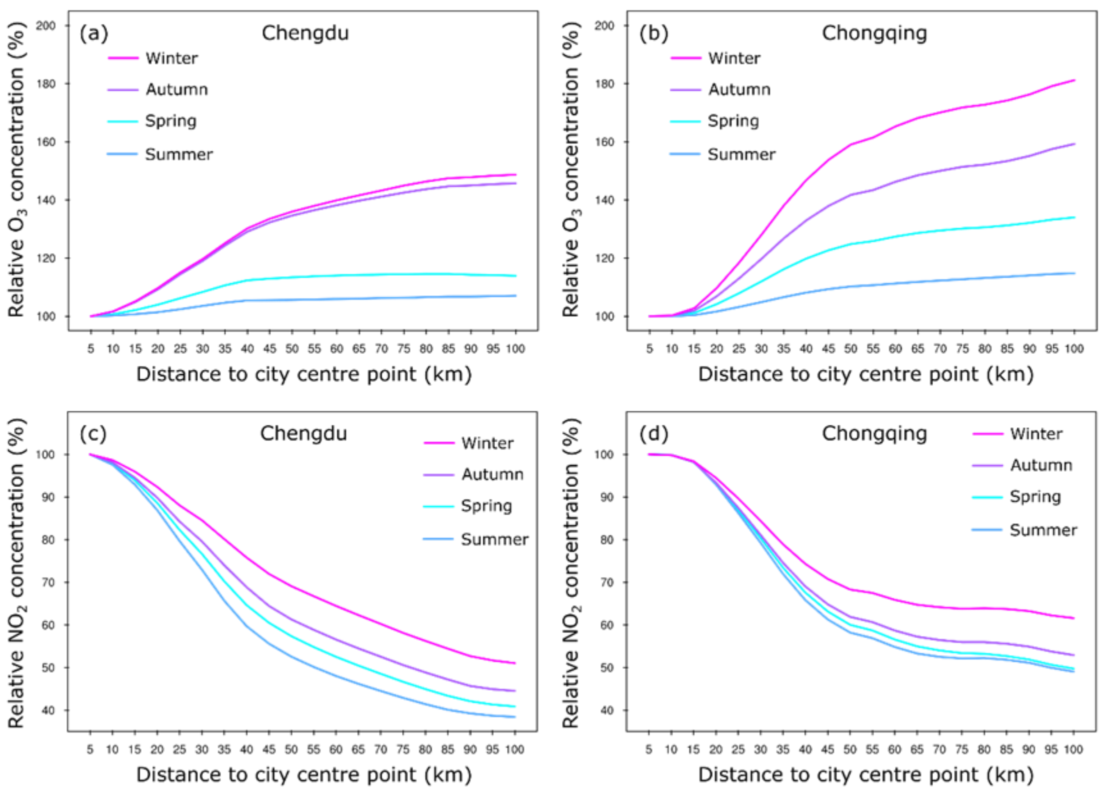

Figure 8: Relative O_3 and NO_2 concentrations along with the core area distance in Chengdu (a, c) and Chongqing (b, d), during 2013-2019. The average value within a 5-km radius centered to the city core area is used as the reference value.

https://doi.org/10.5194/egusphere-2024-3180
Preprint. Discussion started: 6 December 2024

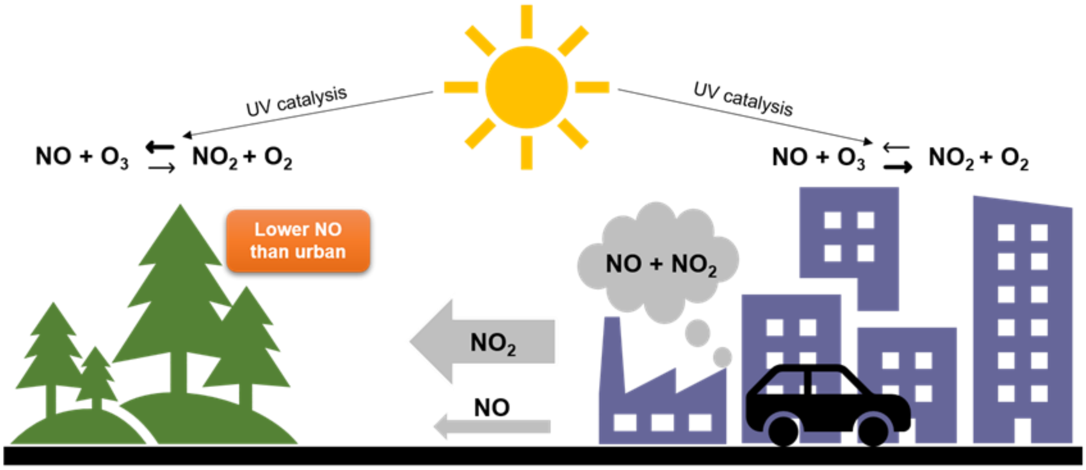

Figure 9: Conceptional schema for the urban ozone trap phenomenon. The thicker arrow in the reaction formula indicates the dominating direction of the atmospheric chemical reaction. The thicker grey arrow indicates a higher proportion of atmospheric NO_2 transported from urban to rural regions compared to NO.

3.3 Possible causes for the ozone trap disparity in strength

The NO_x emissions in urban areas include NO_2 and NO (Zhou et al., 2014). Upon initial NO_x emission into the atmosphere, the abundant NO in NO_x rapidly initiates NO titration, leading to O_3 trapping. During transport to non-urban areas, the titration process depletes most of the NO in NO_x, resulting in a higher proportion of NO_2 and subsequently slowing down NO titration. Hence, due to persistent NO_x emissions in highly urbanized regions, the spatial pattern of the urban O_3 trap takes shape. Thus, we here illustrate a brief mechanism for the urban O_3 trapping (**Figure 9**). To assess the chemical condition, we collected observations of NO_2 and HCHO from the Sentinel-5P. The spatial patterns of NO_2 closely align between satellite observation and the CAQRA dataset (**Figure A5a-d**). Indeed, the satellite NO_2 can only capture the concentration for the whole atmospheric column, while the CAQRA data characterizes near surface concentration. In terms of the satellite observation of formaldehyde from Sentinel-5P, there are hardly any featured spatial patterns for HCHO over the study area (Figure A**5e, f**).

For the O_3 levels among seasons, the photolysis of NO_x-VOCs is ubiquitously stronger in summer due to the ultra-violet (UV) radiation is more available. However, Chongqing is a less urbanized city than Chengdu but has a deeper O_3 trap. Since UV catalysis is one of the potential drivers of O_3 production, other factors should contribute to the difference in solar radiation between Chongqing and Chengdu. Here, we collected site observations of atmospheric visibility and sunshine hours in Chengdu and Chongqing, as these meteorological factors can directly impact the solar radiation reaching the near-surface atmosphere (**Figure 10**). In the study period, atmospheric visibility in Chongqing is at least 20% lower than in Chengdu in all seasons except for summer. It's worth noting that Chongqing is commonly referred to as the 'fog city', a name that has been rumored since ancient times across southwest China. The lowest winter atmospheric visibility in Chongqing (less than 2500 m) and the shortest winter sunshine duration (barely over 1 hour) can contribute to the intense O_3

https://doi.org/10.5194/egusphere-2024-3180
Preprint. Discussion started: 6 December 2024

trapping in winter Chongqing. As for aerosol impacts on radiation, we collected satellite observations from Sentinel-5P to assess the ultraviolet aerosol absorbing. As depicted in the patterns of the ultraviolet absorbing aerosol index (UVAI), UVAI values are globally negative in all seasons (**Figure A7**). This indicates that non-UV-absorbing aerosols are predominant in the Sichuan Basin. Further, as the results of relative concentration in UVAI showed, the concentration of non-UV-absorbing aerosol in the core urban area is lower than in rural. However, the urban-rural gradients of UVAI did not show as high levels as those of ozone or nitrogen dioxide (**Figure A8**). Given the above, the aerosol impacts on the radiation (UV catalysis) are not consistent to the pattern of ozone trap. Further, we presented the combination of land surface temperature (LST) and near-surface wind (**Figure 11**). The main difference between Chengdu and Chongqing appears at night time, which is Chongqing has prominently lower wind speed than Chengdu. Especially, night time wind speed in Chengdu/Chongqing is 1.02/0.40 m s^{-1} and 0.46/0.18 m s^{-1} in 2018 and 2019, respectively. Upon closer examination of the LST in Chengdu and Chongqing (**Figure A6**), the spatial pattern of wind is hardly in line with the urban heat island. From a perspective of atmospheric circulation, the dominant circulation pattern over the Sichuan Basin is controlled by a larger-scale system instead of the in-situ heat pattern of the urban area. Ultimately, the meteorological conditions align more closely with the ozone trap pattern rather than the chemical condition.

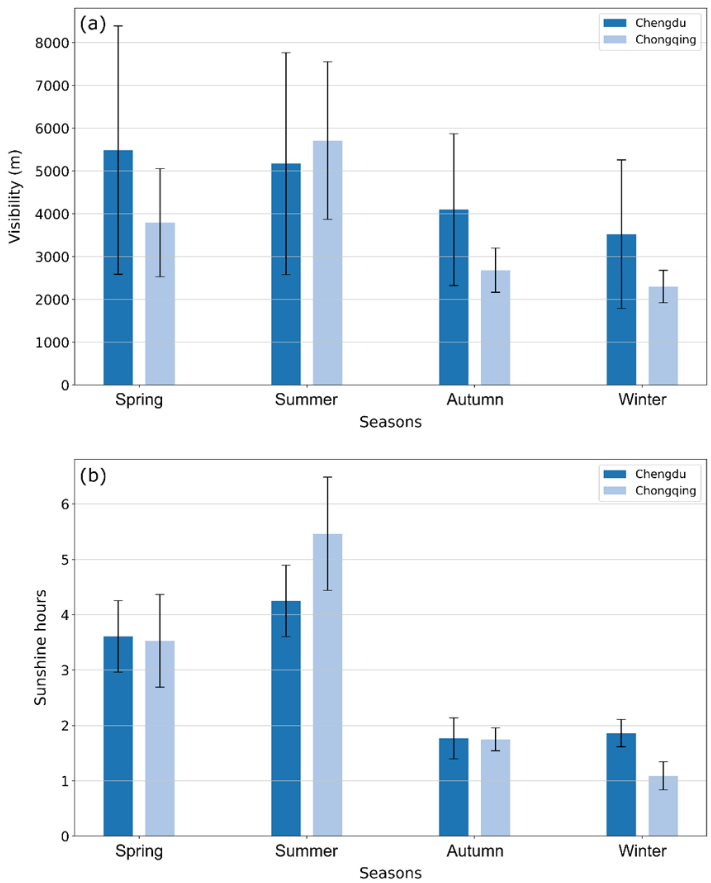

https://doi.org/10.5194/egusphere-2024-3180
Preprint. Discussion started: 6 December 2024

Figure 10: Meteorological conditions from ground auto stations in Chengdu and Chongqing over seasons during 2013-2019. (a) Atmospheric minimum visibility. (b) Daily averaged sunshine duration. Error bars represent one standard deviation of the yearly series.

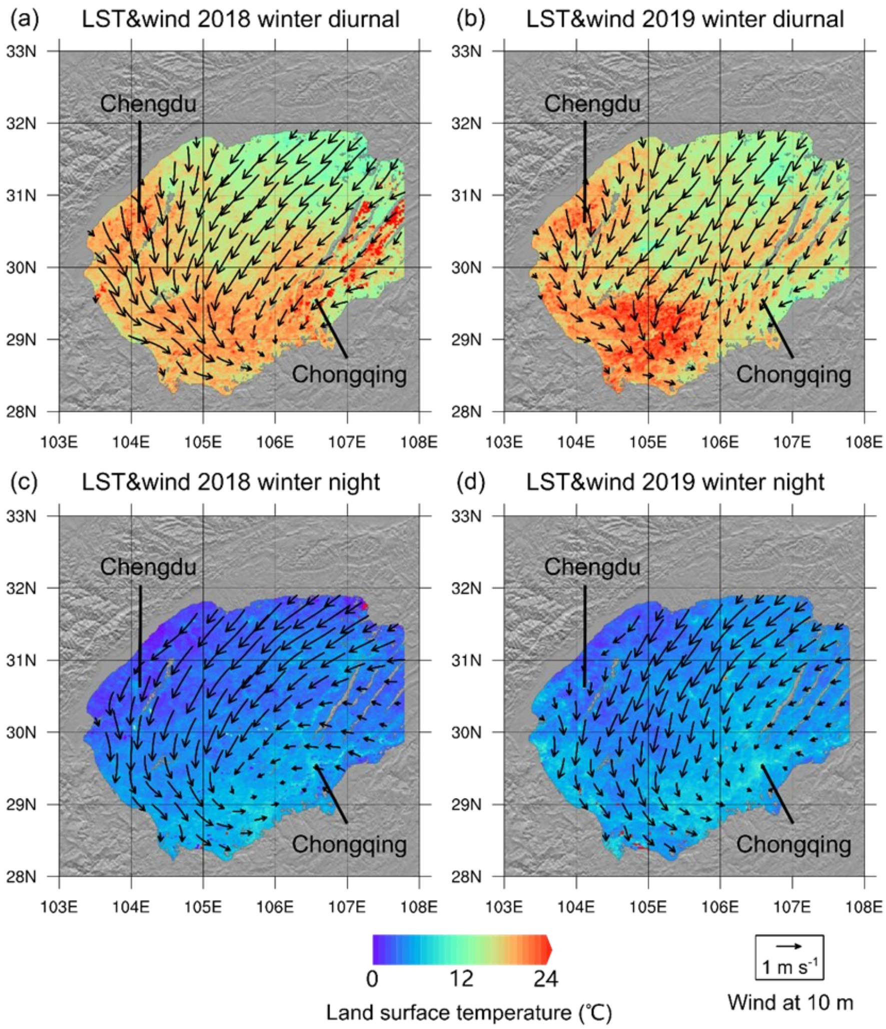

Figure 11: Land surface temperature and 10 m wind from MODIS Aqua and ERA5-Land.

4. Discussion

More than the UV catalysis, many other factors could modulate the reaction balance between NO titration and O_3 production such as the atmospheric concentration of particulate matter (PM) or volatile organic compounds (VOCs) (Jin et al., 2020). As we explored the seasonal spatial patterns of $PM_{2.5}$ (**Figure A2**) and PM_{10} (**Figure A3**) during the study period, the winter PM is notably higher in the study area. From spring to winter, the averaged $PM_{2.5}/PM_{10}$ are 46.4/73.3 μg m^{-3}, 32.2/49.8 μg m^{-3}, 41.3/61.9 μg m^{-3}, and 82.3/114.2 μg m^{-3}, respectively. Further, $PM_{2.5}$ and PM_{10} levels in the urban core area of Chongqing are

https://doi.org/10.5194/egusphere-2024-3180
Preprint. Discussion started: 6 December 2024

lower than those in Chengdu. In Chengdu, $PM_{2.5}/PM_{10}$ levels in spring, summer, autumn, and winter are 59.9/ 105.3 μg m^{-3}, 36.9/ 62.7 μg m^{-3}, 49.8/ 80.4 μg m^{-3}, 102.9/ 150.9 μg m^{-3}, while in Chongqing are 44.7/ 73.5 μg m^{-3}, 33.1/ 54.8 μg m^{-3}, 46.5/ 69.5 μg m^{-3}, 82.2/113.0 μg m^{-3}, respectively. Considering that the core area O_3 levels in Chongqing are lower than those in Chengdu, it is unlikely that the high PM_x played a primary role in enhancing O_3 trapping. Indeed, the background atmospheric circulations also have influences on ground O_3. Through altering the cloud-cover fraction and UV radiation, the Madden–Julian Oscillation has a macroscopic modulation on surface O_3 in a tropical city located on the east coast of the Pacific Ocean (Barrett and Raga, 2016). In north China, typical weather patterns related to temperature, humidity, and circulation are found to facilitate O_3 pollution events, technically, a weather pattern index can capture nearly 80% of the observed events (Gong and Liao, 2019). Moreover, as previous studies demonstrated, there are usually VOCs-limited conditions in China's urban regions while NO_x-limited conditions in rural (Jin and Holloway, 2015). In the Sichuan Basin, observed average $PM_{2.5}$ level in summer decreased by 39% during 2013-2017 (Li et al., 2019).

Based on the analysis of surface air mass transportation, a previous study revealed that the Tibetan Plateau could transmit O_3 to adjacent cities near the western margin of the Sichuan Basin (Zhao et al., 2019). This replenishment of O_3 from the western highlands may weaken the urban-rural O_3 gradient in Chengdu. Moreover, Modelling-based studies also demonstrated the significance of horizontal O_3 advection, in high O_3 episodes, transportation from upstream regions contributed 45% to the pollution across the Chengdu plain (Yang et al., 2020; 2021). However, in our study, urban O_3 trapping is characterized by a 7-year-long averaged estimation, providing a spatial pattern in normal status. Hence, short-term in-situ transportation perturbations are unlikely to have a pronounced impact. As a 6-year-long (2015-2020) study on O_3 and $PM_{2.5}$ across China's main city clusters showed, there are decreasing trends in $PM_{2.5}$ while increases in O_3. Specifically, $PM_{2.5}$ decreased by -2.8 μg m^{-3} yr^{-1}, and O_3 decreased by 2.1 μg m^{-3} yr^{-1} (Deng et al., 2022). In combination with the enhanced seasonality of O_3 (Hayashida et al., 2018), the spatial inconsistency of surface O_3 is more likely to intensify, suggesting that the urban-rural O_3 gradient (or urban O_3 trapping) in the Sichuan Basin has the potential to strengthen. Thus, when the ambient O_3 level in rural regions is further increased, O_3 exposure will pose a more serious threat to crops and vegetation (Ashmore, 2005; Grulke and Heath, 2020). This is especially effective for the urban clusters in our study region, which are surrounded by large areas of croplands (**Figure 1b**).

In contrast to the response of O_3 to sudden emission reductions (Deroubaix et al., 2021), the spatial patterns of O_3 level in our study area exhibited a normal status. Except for Chengdu and Chongqing, other smaller cities with lower urbanized levels did not exhibit comparable O_3 traps in the study area. However theoretically, there should a discernible urban-rural gradient in O_3 levels due to the disparity in emission between urban and rural regions (Munir et al., 2013). Thus, it is likely that the O_3 trapping in megacities offset, and even overrode the spatial pattern of urban-rural gradient in these neighboring smaller cities.

Using a 7-year average, our analysis reveals O_3 traps, not just urban-rural gradients, in near-surface O_3 levels within the two megacities of the Sichuan Basin. These findings help us understand the surface O_3 pattern and its drivers, offering a foundation for assessing future O_3 pollution threats.

5. Conclusion

We used the satellite-based ISA data and site-based air quality reanalysis to evaluate the response of the ground surface O_3 and NO_2 to different urbanization levels during 2013-2019 in the Sichuan Basin. In terms of the normal spatial pattern, O_3 exhibits a negative correlation with the ISA fraction, whereas NO_2 shows the opposite trend. Analyzing the O_3 spatial pattern, we identified two low centers near the city cores of Chengdu and Chongqing. Typically, in winter, the O_3 level in the urban core area of Chengdu/Chongqing is 16.4/22.1 μg m^{-3}, compared to the study region average of 35.7 μg m^{-3}. Next, we used radius distance bins to characterize the urban-rural gradients of the O_3 level, revealed a deeper O_3 trap in Chongqing with lower urbanization level compared to Chengdu. In terms of the most pronounced spatial gradient of O_3 level, whereas in the winter core area in Chongqing is only 16.4 μg m^{-3}, it increases by 8.98% $10km^{-1}$ away from the city core area. Considering that the atmospheric visibility, sunshine duration, and near surface wind are all lower in Chongqing during the cold seasons, aligning with the O_3 trapping pattern, the meteorological conditions are likely primary drivers affecting the balance between NO titration (depleting O_3) and NO_x-VOCs photolysis (producing O_3) in the ambient atmosphere.

Acknowledgments

This study is supported by the Strategic Priority Research Program of the Chinese Academy of Sciences (grant no. XDA23100401). Authors appreciate the Global Multi-resolution Terrain Elevation Data 2010 courtesy of the U.S. Geological Survey.

Code/Data availability

Code/Data are available upon request from the corresponding author.

Author contribution

Chenxi Wang: Writing - Original Draft, Data Curation, Formal analysis
Zheng Jin: Conceptualization, Investigation, Methodology, Visualization, Writing - Review & Editing
Yang Liu: Software, Validation, Resources, Data Curation, Funding acquisition
Mengxin Bai: Resources, Data Curation, Validation
Weijia Wang: Validation, Data Curation
Yingzhuo Yu: Software, Supervision
Liantang Deng: Supervision

Competing interests

The contact author has declared that none of the authors has any competing interests.

References

Anenberg Susan, C., Schwartz, J., Shindell, D., Amann, M., Faluvegi, G., Klimont, Z., Janssens-Maenhout, G., Pozzoli, L., Van Dingenen, R., Vignati, E., Emberson, L., Muller Nicholas, Z., West, J. J., Williams, M., Demkine, V., Hicks, W. K., Kuylenstierna, J., Raes, F., and Ramanathan, V.: Global Air Quality and Health Co-benefits of Mitigating Near-Term Climate Change through Methane and Black Carbon Emission Controls, Environmental Health Perspectives, 120, 831-839, https://doi.org/10.1289/ehp.1104301, 2012.

Ashmore, M. R.: Assessing the future global impacts of ozone on vegetation, Plant, Cell & Environment, 28, 949-964, https://doi.org/10.1111/j.1365-3040.2005.01341.x, 2005.

Atkinson Richard, W., Yu, D., Armstrong Ben, G., Pattenden, S., Wilkinson, P., Doherty Ruth, M., Heal Mathew, R., and Anderson, H. R.: Concentration–Response Function for Ozone and Daily Mortality: Results from Five Urban and Five Rural U.K. Populations, Environmental Health Perspectives, 120, 1411-1417, https://10.1289/ehp.1104108, 2012.

Barrett, B. S. and Raga, G. B.: Variability of winter and summer surface ozone in Mexico City on the intraseasonal timescale, Atmospheric Chemistry and Physics, 16, 15359-15370, https://10.5194/acp-16-15359-2016, 2016.

Betancourt-Odio, A., Valencia, D., Soffritti, M., and Budría, S.: An analysis of ozone pollution by using functional data: rural and urban areas of the Community of Madrid, Environmental Monitoring and Assessment, 193, 401, https://doi.org/10.1007/s10661-021-09180-1, 2021.

Cao, B., Wang, X., Ning, G., Yuan, L., Jiang, M., Zhang, X., and Wang, S.: Factors influencing the boundary layer height and their relationship with air quality in the Sichuan Basin, China, Science of The Total Environment, 727, 138584, https://doi.org/10.1016/j.scitotenv.2020.138584, 2020.

Danielson, J. J. and Gesch, D. B.: Global multi-resolution terrain elevation data 2010 (GMTED2010), U.S. Geological Survey, 26, https://doi.org/10.3133/ofr20111073, 2011.

Deng, C., Tian, S., Li, Z., and Li, K.: Spatiotemporal characteristics of PM2.5 and ozone concentrations in Chinese urban clusters, Chemosphere, 295, 133813, https://doi.org/10.1016/j.chemosphere.2022.133813, 2022.

Deroubaix, A., Brasseur, G., Gaubert, B., Labuhn, I., Menut, L., Siour, G., and Tuccella, P.: Response of surface ozone concentration to emission reduction and meteorology during the COVID-19 lockdown in Europe, Meteorological Applications, 28, e1990, https://doi.org/10.1002/met.1990, 2021.

Dueñas, C., Fernández, M. C., Cañete, S., Carretero, J., and Liger, E.: Analyses of ozone in urban and rural sites in Málaga (Spain), Chemosphere, 56, 631-639, https://doi.org/10.1016/j.chemosphere.2004.04.013, 2004.

Fang, C., Tan, X., Zhong, Y., and Wang, J.: Research on the Temporal and Spatial Characteristics of Air Pollutants in Sichuan Basin, Atmosphere, 12, https://10.3390/atmos12111504, 2021.

Friedl, M. A. and Sulla-Menashe, D.: MCD12Q1 MODIS/Terra+Aqua Land Cover Type Yearly L3 Global 500 m SIN Grid V006 Data Set [dataset], https://doi.org/10.5067/MODIS/MCD12Q1.006, 2019.

Gong, C. and Liao, H.: A typical weather pattern for ozone pollution events in North China, Atmospheric Chemistry and Physics, 19, 13725-13740, https://10.5194/acp-19-13725-2019, 2019.

Gong, P., Li, X., Wang, J., Bai, Y., Chen, B., Hu, T., Liu, X., Xu, B., Yang, J., Zhang, W., and Zhou, Y.: Annual maps of global artificial impervious area (GAIA) between 1985 and 2018, Remote Sensing of Environment, 236, 111510, https://doi.org/10.1016/j.rse.2019.111510, 2020.

Grulke, N. E. and Heath, R. L.: Ozone effects on plants in natural ecosystems, Plant Biology, 22, 12-37, https://doi.org/10.1111/plb.12971, 2020.

Hagenbjörk, A., Malmqvist, E., Mattisson, K., Sommar, N. J., and Modig, L.: The spatial variation of O3, NO, NO2 and NOxand the relation between them in two Swedish cities, Environmental Monitoring and Assessment, 189, 161, https://10.1007/s10661-017-5872-z, 2017.

Hayashida, S., Kajino, M., Deushi, M., Sekiyama, T. T., and Liu, X.: Seasonality of the lower tropospheric ozone over China observed by the Ozone Monitoring Instrument, Atmospheric Environment, 184, 244-253, https://doi.org/10.1016/j.atmosenv.2018.04.014, 2018.

Im, U., Incecik, S., Guler, M., Tek, A., Topcu, S., Unal, Y. S., Yenigun, O., Kindap, T., Odman, M. T., and Tayanc, M.: Analysis of surface ozone and nitrogen oxides at urban, semi-rural and rural sites in Istanbul, Turkey, Science of The Total Environment, 443, 920-931, https://doi.org/10.1016/j.scitotenv.2012.11.048, 2013.

Jin, X. and Holloway, T.: Spatial and temporal variability of ozone sensitivity over China observed from the Ozone Monitoring Instrument, Journal of Geophysical Research: Atmospheres, 120, 7229-7246, https://doi.org/10.1002/2015JD023250, 2015.

Jin, X., Fiore, A., Boersma, K. F., Smedt, I. D., and Valin, L.: Inferring Changes in Summertime Surface Ozone–NOx–VOC Chemistry over U.S. Urban Areas from Two Decades of Satellite and Ground-Based Observations, Environmental Science & Technology, 54, 6518-6529, https://10.1021/acs.est.9b07785, 2020.

Kleinman, L. I.: Low and high NOx tropospheric photochemistry, Journal of Geophysical Research: Atmospheres, 99, 16831-16838, https://doi.org/10.1029/94JD01028, 1994.

Kong, L., Tang, X., Zhu, J., Wang, Z., Li, J., Wu, H., Wu, Q., Chen, H., Zhu, L., Wang, W., Liu, B., Wang, Q., Chen, D., Pan, Y., Song, T., Li, F., Zheng, H., Jia, G., Lu, M., Wu, L., and Carmichael, G. R.: A 6-year-long (2013–2018) high-resolution air quality reanalysis dataset in China based on the assimilation of surface observations from CNEMC, Earth System Science Data, 13, 529-570, https://10.5194/essd-13-529-2021, 2021.

Lelieveld, J. and Dentener, F. J.: What controls tropospheric ozone?, Journal of Geophysical Research: Atmospheres, 105, 3531-3551, https://doi.org/10.1029/1999JD901011, 2000.

Lelieveld, J., Evans, J. S., Fnais, M., Giannadaki, D., and Pozzer, A.: The contribution of outdoor air pollution sources to premature mortality on a global scale, Nature, 525, 367-371, https://10.1038/nature15371, 2015.

Li, K., Jacob Daniel, J., Liao, H., Shen, L., Zhang, Q., and Bates Kelvin, H.: Anthropogenic drivers of 2013–2017 trends in summer surface ozone in China, Proceedings of the National Academy of Sciences, 116, 422-427, https://10.1073/pnas.1812168116, 2019.

Li, X., Gong, P., Zhou, Y., Wang, J., Bai, Y., Chen, B., Hu, T., Xiao, Y., Xu, B., Yang, J., Liu, X., Cai, W., Huang, H., Wu, T., Wang, X., Lin, P., Li, X., Chen, J., He, C., Li, X., Yu, L., Clinton, N., and Zhu, Z.: Mapping global urban boundaries from the global artificial impervious area (GAIA) data, Environmental Research Letters, 15, 094044, https://10.1088/1748-9326/ab9be3, 2020.

Liao, T., Gui, K., Jiang, W., Wang, S., Wang, B., Zeng, Z., Che, H., Wang, Y., and Sun, Y.: Air stagnation and its impact on air quality during winter in Sichuan and Chongqing, southwestern China, Science of The Total Environment, 635, 576-585, https://doi.org/10.1016/j.scitotenv.2018.04.122, 2018.

Liu, R., Ma, Z., Liu, Y., Shao, Y., Zhao, W., and Bi, J.: Spatiotemporal distributions of surface ozone levels in China from 2005 to 2017: A machine learning approach, Environment International, 142, 105823, https://doi.org/10.1016/j.envint.2020.105823, 2020.

Liu, W., Hegglin, M. I., Checa-Garcia, R., Li, S., Gillett, N. P., Lyu, K., Zhang, X., and Swart, N. C.: Stratospheric ozone depletion and tropospheric ozone increases drive Southern Ocean interior warming, Nature Climate Change, 12, 365-372, https://10.1038/s41558-022-01320-w, 2022.

Lu, X., Hong, J., Zhang, L., Cooper, O. R., Schultz, M. G., Xu, X., Wang, T., Gao, M., Zhao, Y., and Zhang, Y.: Severe Surface Ozone Pollution in China: A Global Perspective, Environmental Science & Technology Letters, 5, 487-494, https://10.1021/acs.estlett.8b00366, 2018.

Mickley, L. J., Murti, P. P., Jacob, D. J., Logan, J. A., Koch, D. M., and Rind, D.: Radiative forcing from tropospheric ozone calculated with a unified chemistry-climate model, Journal of Geophysical Research: Atmospheres, 104, 30153-30172, https://doi.org/10.1029/1999JD900439, 1999.

Monks, P. S., Archibald, A. T., Colette, A., Cooper, O., Coyle, M., Derwent, R., Fowler, D., Granier, C., Law, K. S., Mills, G. E., Stevenson, D. S., Tarasova, O., Thouret, V., von Schneidemesser, E., Sommariva, R., Wild, O., and Williams, M. L.: Tropospheric ozone and its precursors from the urban to the global scale from air quality to short-lived climate forcer, Atmospheric Chemistry and Physics, 15, 8889-8973, https://10.5194/acp-15-8889-2015, 2015.

Munir, S., Chen, H., and Ropkins, K.: Quantifying temporal trends in ground level ozone concentration in the UK, Science of The Total Environment, 458-460, 217-227, https://doi.org/10.1016/j.scitotenv.2013.04.045, 2013.

Muñoz-Sabater, J., Dutra, E., Agustí-Panareda, A., Albergel, C., Arduini, G., Balsamo, G., Boussetta, S., Choulga, M., Harrigan, S., Hersbach, H., Martens, B., Miralles, D. G., Piles, M., Rodríguez-Fernández, N. J., Zsoter, E., Buontempo, C., and Thépaut, J. N.: ERA5-Land: a state-of-the-art global reanalysis dataset for land applications, Earth Syst. Sci. Data, 13, 4349-4383, https://doi.org/10.5194/essd-13-4349-2021, 2021.

Murphy, J. G., Day, D. A., Cleary, P. A., Wooldridge, P. J., Millet, D. B., Goldstein, A. H., and Cohen, R. C.: The weekend effect within and downwind of Sacramento – Part 1: Observations of ozone, nitrogen oxides, and VOC reactivity, Atmospheric Chemistry and Physics, 7, 5327-5339, https://10.5194/acp-7-5327-2007, 2007.

Ning, G., Yim, S. H. L., Yang, Y., Gu, Y., and Dong, G.: Modulations of synoptic and climatic changes on ozone pollution and its health risks in mountain-basin areas, Atmospheric Environment, 240, 117808, https://doi.org/10.1016/j.atmosenv.2020.117808, 2020.

Sillman, S.: The relation between ozone, NOx and hydrocarbons in urban and polluted rural environments, Atmospheric Environment, 33, 1821-1845, https://doi.org/10.1016/S1352-2310(98)00345-8, 1999.

Stasiuk, W. N. and Coffey, P. E.: Rural and Urban Ozone Relationships In New York State, Journal of the Air Pollution Control Association, 24, 564-568, https://10.1080/00022470.1974.10469941, 1974.

Tai, A. P. K., Martin, M. V., and Heald, C. L.: Threat to future global food security from climate change and ozone air pollution, Nature Climate Change, 4, 817-821, https://10.1038/nclimate2317, 2014.

Unger, N., Shindell Drew, T., Koch Dorothy, M., and Streets David, G.: Cross influences of ozone and sulfate precursor emissions changes on air quality and climate, Proceedings of the National Academy of Sciences, 103, 4377-4380, https://10.1073/pnas.0508769103, 2006.

Veefkind, J. P., Aben, I., McMullan, K., Förster, H., de Vries, J., Otter, G., Claas, J., Eskes, H. J., de Haan, J. F., Kleipool, Q., van Weele, M., Hasekamp, O., Hoogeveen, R., Landgraf, J., Snel, R., Tol, P., Ingmann, P., Voors, R., Kruizinga, B., Vink, R., Visser, H., and Levelt, P. F.: TROPOMI on the ESA Sentinel-5 Precursor: A GMES mission for global observations of the atmospheric composition for climate, air quality and ozone layer applications, Remote Sensing of Environment, 120, 70-83, https://doi.org/10.1016/j.rse.2011.09.027, 2012.

Wang, T., Xue, L., Brimblecombe, P., Lam, Y. F., Li, L., and Zhang, L.: Ozone pollution in China: A review of concentrations, meteorological influences, chemical precursors, and effects, Science of The Total Environment, 575, 1582-1596, https://doi.org/10.1016/j.scitotenv.2016.10.081, 2017.

Wang, Y., Shen, L., Wu, S., Mickley, L., He, J., and Hao, J.: Sensitivity of surface ozone over China to 2000–2050 global changes of climate and emissions, Atmospheric Environment, 75, 374-382, https://doi.org/10.1016/j.atmosenv.2013.04.045, 2013.

Wu, K., Wang, Y., Qiao, Y., Liu, Y., Wang, S., Yang, X., Wang, H., Lu, Y., Zhang, X., and Lei, Y.: Drivers of 2013–2020 ozone trends in the Sichuan Basin, China: Impacts of meteorology and precursor emission changes, Environmental Pollution, 300, 118914, https://doi.org/10.1016/j.envpol.2022.118914, 2022.

Yan, Y., Lin, J., Pozzer, A., Kong, S., and Lelieveld, J.: Trend reversal from high-to-low and from rural-to-urban ozone concentrations over Europe, Atmospheric Environment, 213, 25-36, https://doi.org/10.1016/j.atmosenv.2019.05.067, 2019.

Yang, X., Wu, K., Lu, Y., Wang, S., Qiao, Y., Zhang, X., Wang, Y., Wang, H., Liu, Z., Liu, Y., and Lei, Y.: Origin of regional springtime ozone episodes in the Sichuan Basin, China: Role of synoptic forcing and regional transport, Environmental Pollution, 278, 116845, https://doi.org/10.1016/j.envpol.2021.116845, 2021.

Yang, X., Wu, K., Wang, H., Liu, Y., Gu, S., Lu, Y., Zhang, X., Hu, Y., Ou, Y., Wang, S., and Wang, Z.: Summertime ozone pollution in Sichuan Basin, China: Meteorological conditions, sources and process analysis, Atmospheric Environment, 226, 117392, https://doi.org/10.1016/j.atmosenv.2020.117392, 2020.

Yue, X., Unger, N., Harper, K., Xia, X., Liao, H., Zhu, T., Xiao, J., Feng, Z., and Li, J.: Ozone and haze pollution weakens net primary productivity in China, Atmospheric Chemistry and Physics, 17, 6073-6089, https://10.5194/acp-17-6073-2017, 2017.

Zhang, X., Zhao, L., Cheng, M., Wu, X., and Chen, D.: Urban ozone sink inferred from surface measurements in China, Journal of Cleaner Production, 253, 119881, https://doi.org/10.1016/j.jclepro.2019.119881, 2020.

Zhang, Y., Yin, P., Li, X., Niu, Q., Wang, Y., Cao, W., Huang, J., Chen, H., Yao, X., Yu, L., and Li, B.: The divergent response of vegetation phenology to urbanization: A case study of Beijing city, China, Science of The Total Environment, 803, 150079, https://doi.org/10.1016/j.scitotenv.2021.150079, 2022.

Zhao, S., Yu, Y., Qin, D., Yin, D., Dong, L., and He, J.: Analyses of regional pollution and transportation of PM2.5 and ozone in the city clusters of Sichuan Basin, China, Atmospheric Pollution Research, 10, 374-385, https://doi.org/10.1016/j.apr.2018.08.014, 2019.

Zhao, S., Yu, Y., Yin, D., Qin, D., He, J., and Dong, L.: Spatial patterns and temporal variations of six criteria air pollutants during 2015 to 2017 in the city clusters of Sichuan Basin, China, Science of The Total Environment, 624, 540-557, https://doi.org/10.1016/j.scitotenv.2017.12.172, 2018.

Zhou, R., Wang, S., Shi, C., Wang, W., Zhao, H., Liu, R., Chen, L., and Zhou, B.: Study on the Traffic Air Pollution inside and outside a Road Tunnel in Shanghai, China, PLOS ONE, 9, e112195, https://10.1371/journal.pone.0112195, 2014.

https://doi.org/10.5194/egusphere-2024-3180
Preprint. Discussion started: 6 December 2024

Appendix

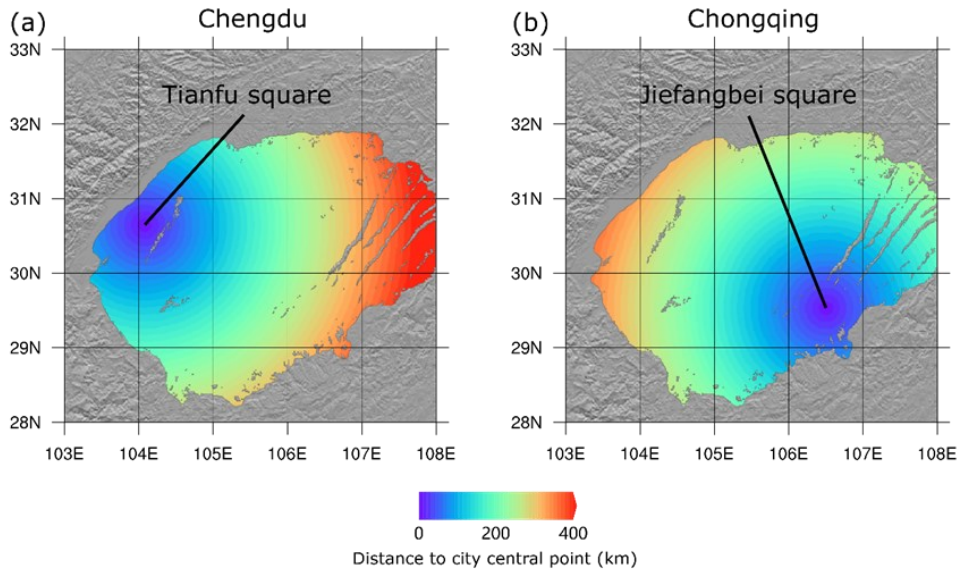

495 **Figure A1: Relative distance from the city core for Chengdu (a) and Chongqing (b) at a horizontal resolution of 1 km × 1 km.**

https://doi.org/10.5194/egusphere-2024-3180
Preprint. Discussion started: 6 December 2024

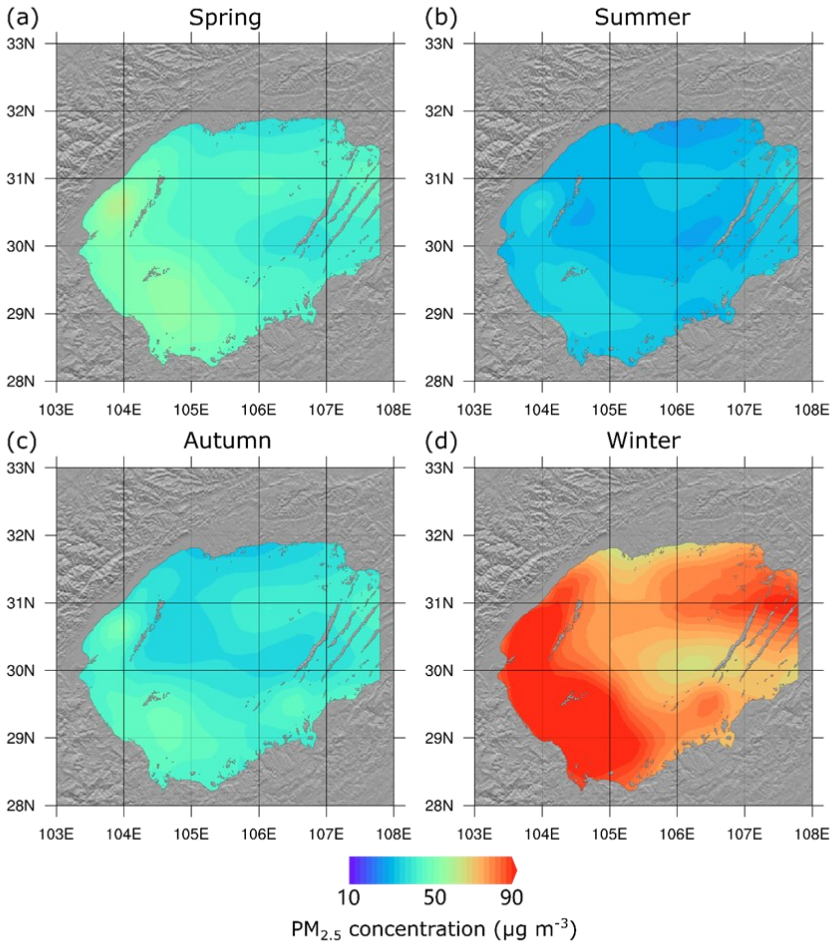

Figure A2: Spatial patterns for $PM_{2.5}$ concentrations over seasons during 2013-2019.

https://doi.org/10.5194/egusphere-2024-3180
Preprint. Discussion started: 6 December 2024

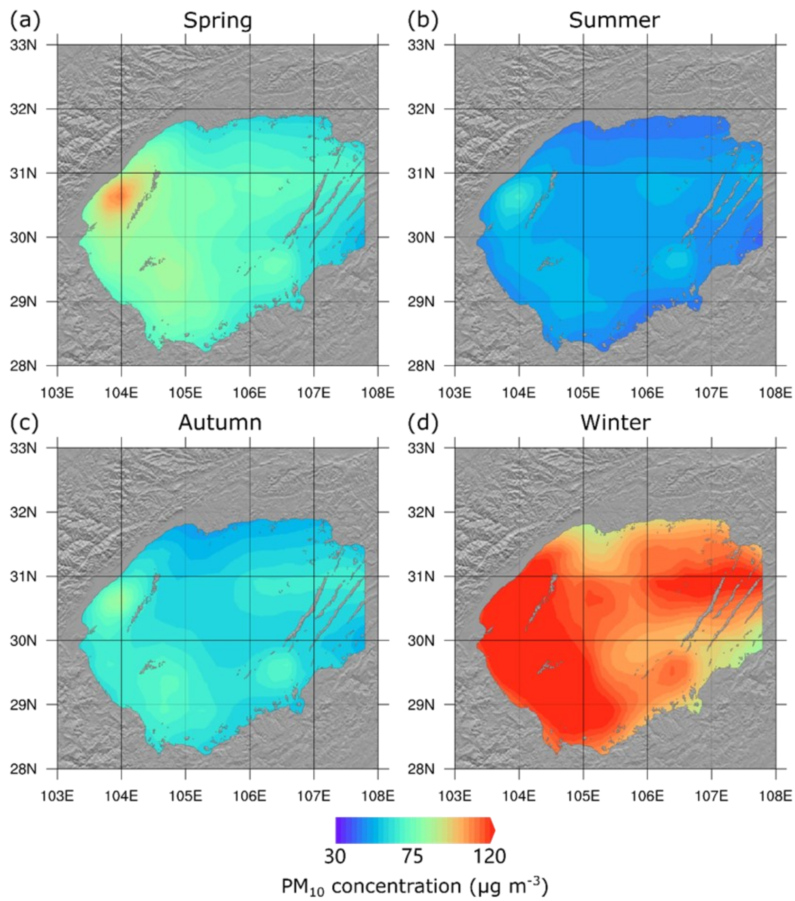

Figure A3: Spatial patterns for PM_{10} concentrations over seasons during 2013-2019.

https://doi.org/10.5194/egusphere-2024-3180
Preprint. Discussion started: 6 December 2024

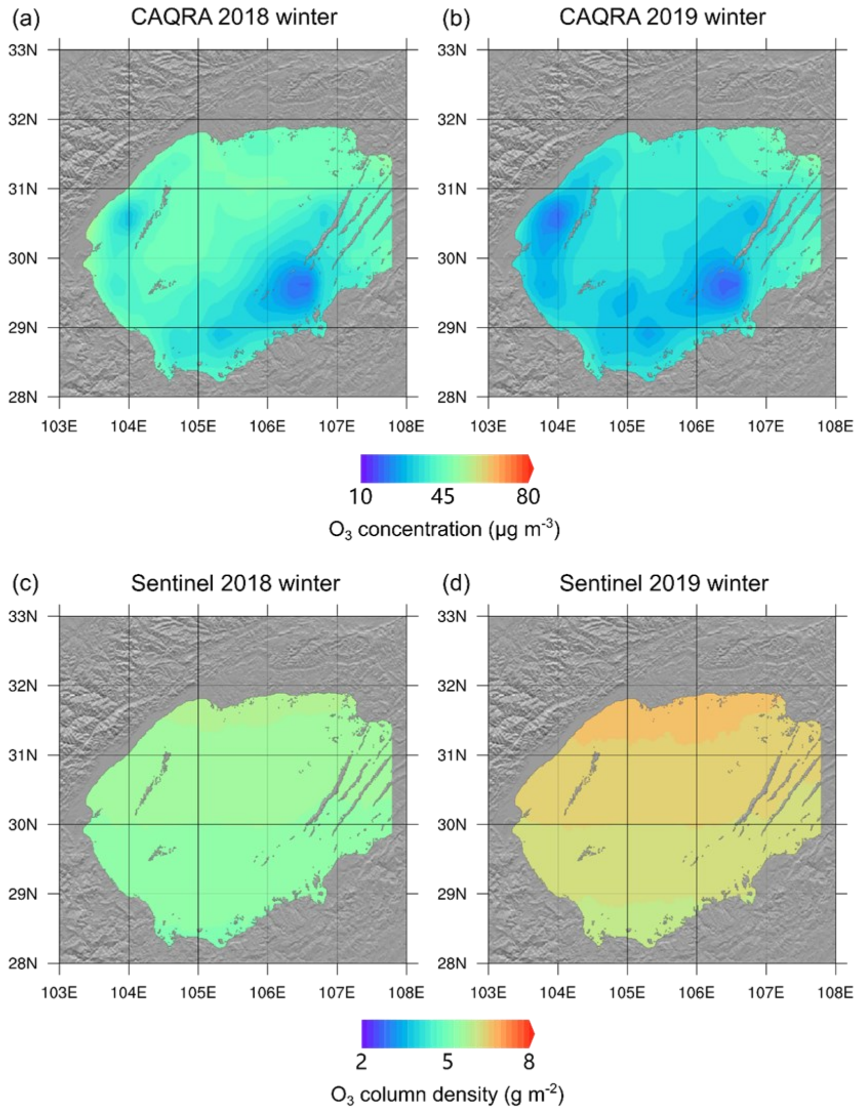

Figure A4: Comparison of winter ozone spatial patterns between CAQRA data and Sentinel-5P observations.

https://doi.org/10.5194/egusphere-2024-3180
Preprint. Discussion started: 6 December 2024

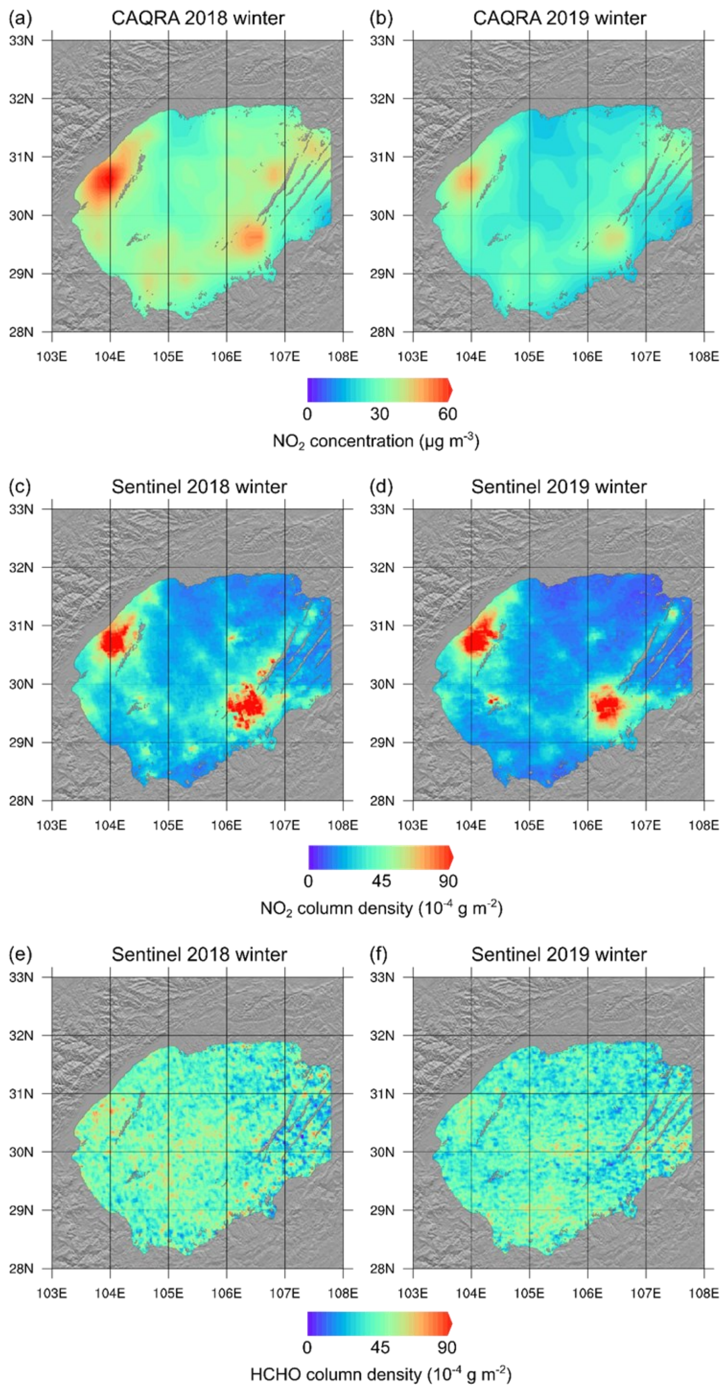

Figure A5: Comparison of winter NO_2 spatial patterns between CAQRA data and Sentinel-5P observations (a-d). HCHO spatial
500 **patterns from Sentinel-5P (e-f).**

https://doi.org/10.5194/egusphere-2024-3180
Preprint. Discussion started: 6 December 2024

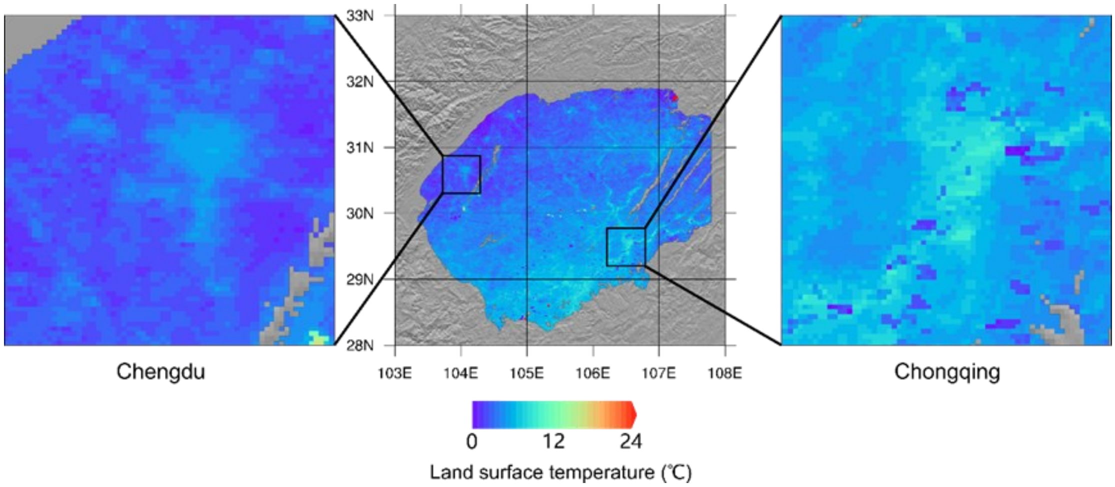

Figure A6: Land surface temperature from MODIS Aqua with zoom-in view to display the pattern of urban heat island over 2018 winter night.

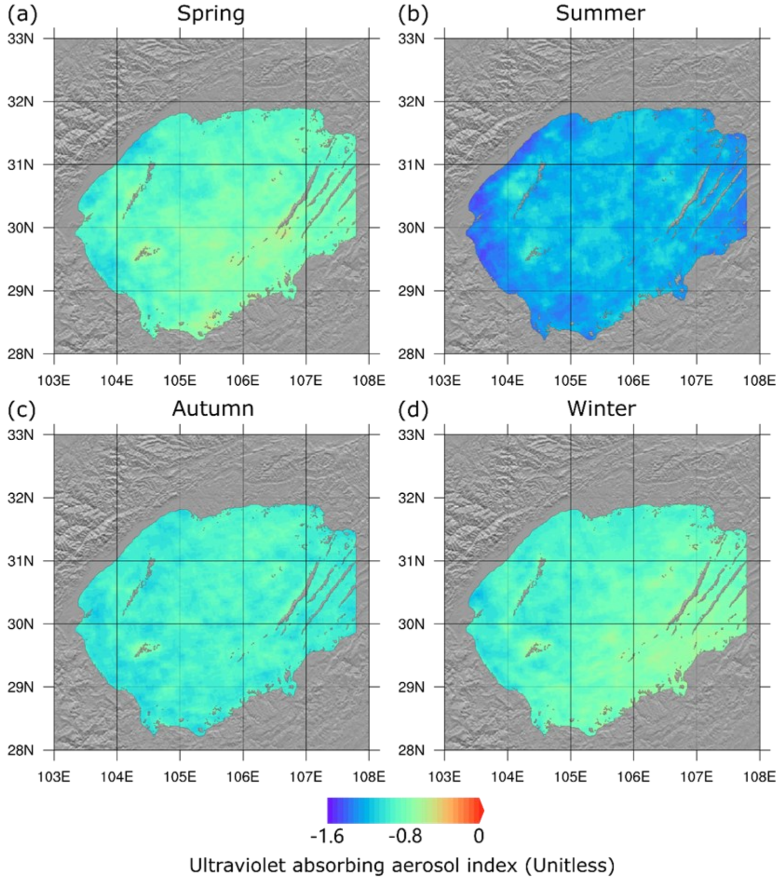

Figure A7: Ultraviolet absorbing aerosol index from Sentinel-5P observations over 2019.

https://doi.org/10.5194/egusphere-2024-3180
Preprint. Discussion started: 6 December 2024

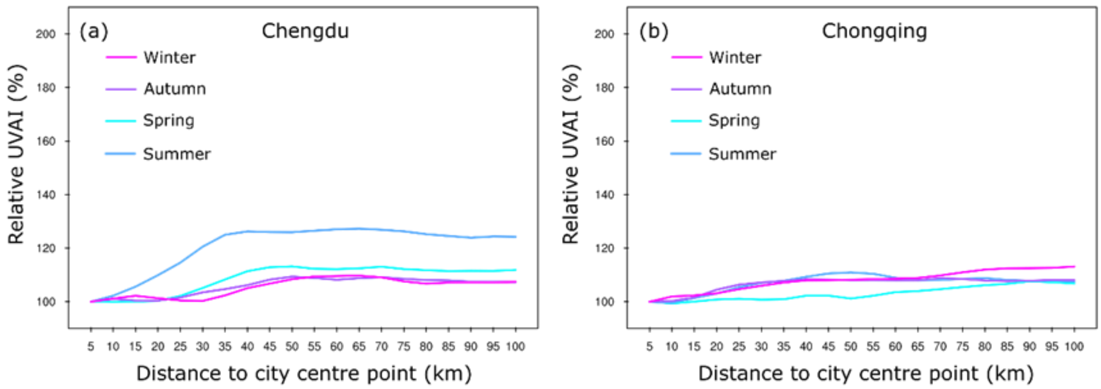

505 **Figure A8: Relative concentration of ultraviolet absorbing aerosol index (UVAI) along with core area distance in Chengdu (a) and Chongqing (b) in 2019. The average value within a 5-km radius centered to the city core area is used as the reference value.**